

# Selectively excited luminescence and magnetic circular dichroism of Cr<sup>4+</sup>-doped YAG and YGG

M. J. Riley

*Department of Chemistry, University of Queensland, St. Lucia 4072, Australia*

E. R. Krausz

*Research School of Chemistry, Australian National University, Canberra 0200, Australia*

N. B. Manson

*Research School of Physical Sciences and Engineering, Australian National University, Canberra 0200, Australia*

B. Henderson

*Cavendish Laboratory, University of Cambridge, Cambridge CB3 0HE, United Kingdom*

(Received 8 September 1998)

Site selective luminescence and magnetic circular dichroism experiments on Cr<sup>4+</sup>-doped yttrium aluminum garnet and yttrium gallium garnet have been made at low temperature. The spectral assignments for these near-IR lasing materials have been made using experimental data and ligand field calculations guided by the known geometry of the lattices. [S0163-1829(99)07003-4]

## I. INTRODUCTION

There has been intense interest in the spectroscopy of Cr<sup>4+</sup> in tetraoxo coordination environments since room-temperature laser operation has been demonstrated in many doped systems. These include Cr<sup>4+</sup> doped into forsterite (Mg<sub>2</sub>SiO<sub>4</sub>),<sup>1</sup> yttrium aluminum garnet (YAG, Y<sub>3</sub>Al<sub>5</sub>O<sub>12</sub>),<sup>2</sup> and yttrium oxyorthosilicate (Y<sub>2</sub>SiO<sub>5</sub>).<sup>3</sup> Recently, an all solid-state Cr<sup>4+</sup>:YAG laser has been used to generate 43-fs pulses.<sup>4</sup> Spectroscopic studies of these systems have established that the Cr<sup>4+</sup> emitting center is fourfold coordinated<sup>5-8</sup> with various degrees of distortion away from exact tetrahedral symmetry. However, there remain puzzling aspects including multiple charge states and site symmetries of the Cr dopant, which have resulted in ambiguous spectral and electronic structural assignments. Here, we present site selective luminescence and magnetic circular dichroism (MCD) spectra of Cr<sup>4+</sup>-doped yttrium aluminum garnet (YAG) and yttrium gallium garnet (YGG). A summary of the problems and many of the spectroscopic results of Cr<sup>4+</sup>:YAG are given in Eilers *et al.*<sup>6</sup> There has been comparatively little work on Cr<sup>4+</sup>:YGG previously published,<sup>7</sup> but the present investigation indicates close similarities to the Cr<sup>4+</sup>:YAG system. Here we interpret the spectra in terms of a detailed ligand field analysis and find that while the guest ion adopts the host geometry, the interelectron repulsion Racah parameter is required to be much smaller than expected.

## II. EXPERIMENT

YAG and YGG are both cubic structures ( $O_h^{10}$ ) that can be written as  $A_3B_2(CO_4)_3$ , where the  $M^{3+}$  cation sites are nominally dodecahedral ( $A=Y$ ), octahedral ( $B=Al, Ga$ ), and tetrahedral ( $C=Al, Ga$ ). The tetrahedral site has exact  $S_4$  symmetry but is  $D_{2d}$  considering only nearest neighbors. The  $D_{2d}$  distorted tetrahedron is elongated, the angle each

bond makes with the elongation axis is reduced from the tetrahedral value of  $54.7^\circ$  by  $\alpha=4.6^\circ$  ( $\alpha=5.2^\circ$ ) for YAG (YGG).<sup>9,10</sup> The crystals of Cr<sup>4+</sup>:YAG and Cr<sup>4+</sup>:YGG were grown at OMRC, University of Strathclyde, Glasgow, UK using a Czochralski crystal puller.<sup>9</sup> Appropriate combinations of powdered components were sintered at 1200 K in a mildly oxidizing atmosphere (N<sub>2</sub>+2%O<sub>2</sub>) before melting in Ir crucibles. Single-crystal boules of typical dimensions 20 mm diameter by 60 mm length were grown onto seed crystals of known orientation that had been previously grown on Ir wires. The CaO/Cr<sub>2</sub>O<sub>3</sub> ratios were chosen to give optimal Cr<sup>4+</sup> concentrations after growth and post-growth processing. In both YAG and YGG the dopant ratio was determined to be 4:1 (CaO:Cr<sub>2</sub>O<sub>3</sub>) by weight, and the total Cr content of the melt  $2.8 \times 10^{19}$  Cr cm<sup>-3</sup>. The boules were subsequently annealed in a N<sub>2</sub>+20%O<sub>2</sub> mixture at 1400 K for 24 h. Spectroscopic assay showed that some 90% of Cr ions occupy the octahedral  $B$  sites as Cr<sup>3+</sup>, with 2% and <1%, respectively of Cr<sup>4+</sup> and Cr<sup>6+</sup> occupying the tetrahedral  $C$  sites.<sup>9</sup> Optical absorption (170–2000 nm) and luminescence (500–2000 nm) studies of these and related crystals show complex overlapping bands associated with (at least) Cr<sup>3+</sup>, Cr<sup>4+</sup>, and Cr<sup>6+</sup> charge states of the active dopant. However, the dominant components of the optical absorption and luminescence spectra are associated with Cr<sup>4+</sup> ions occupying the  $D_{2d}$  distorted tetrahedral  $C$  sites.

Simultaneous MCD and absorption spectra were measured using an Spex 1404 monochromator, photoelastic modulator, Oxford Instruments SM4 cryomagnet, and cooled InSb detector with heterodyne detected modulation in an apparatus described previously.<sup>11</sup> The sample temperature could be varied from 1.5 to 100 K while in a helium gas/liquid environment.

The luminescence spectra were obtained using the same cryostat. Samples were excited with either a cw Ar<sup>+</sup> laser or tunable 5 ns pulsed radiation from a Mirage 500 OPO/OPA driven by a Continuum Powerlite injection seeded YAG la-

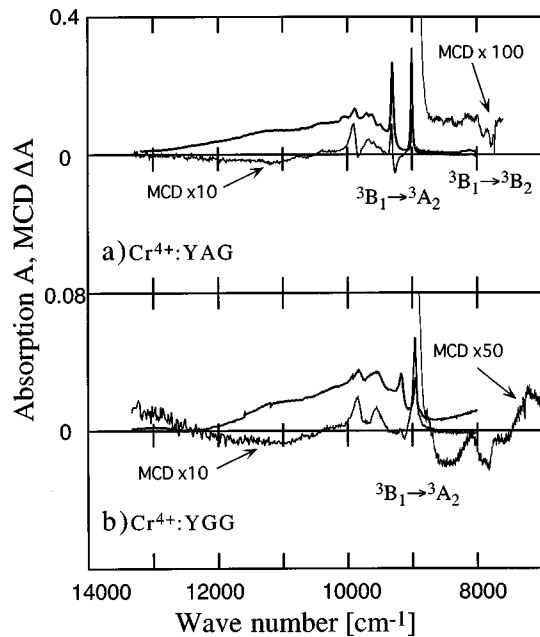


FIG. 1. The near-IR absorption (thicker traces:  $A$ ) and MCD (thinner traces:  $\Delta A$ ) spectra at  $T=1.5$  K and applied field  $B$  of 5 T; of (a)  $\text{Cr}^{4+}:\text{YAG}$  and (b)  $\text{Cr}^{4+}:\text{YGG}$ . Light was propagated down the (001) direction of the cubic crystals.

ser system. Luminescence was detected with an ADC  $\text{LN}_2$ -cooled germanium diode and a Spex 0.75 M monochromator fitted with a grating blazed at  $1.6 \mu\text{m}$ .

### III. RESULTS

The absorption and MCD spectra of  $\text{Cr}^{4+}:\text{YAG}$  and  $\text{Cr}^{4+}:\text{YGG}$  in the near-IR region at 1.5 K are shown in Figs. 1–3. There is a strong ( $\sim 1/T$ ) temperature-dependent decrease of the MCD magnitudes (see Fig. 2). Such  $C$  term type<sup>12</sup> behavior is most often associated with a (quasi)degenerate ground state of the absorbing species.

The MCD spectra taken in the visible region also reveal the presence of  $\text{Cr}^{3+}$  ions (Fig. 3). Distinctive  $R$  lines are seen, with  $26 \text{ cm}^{-1}$  spacing and strong negative MCD features with  $\Delta A/A$  approaching 2 under saturation conditions ( $g\beta B \gg kT$ ). The  $R$  lines occur near  $14550 \text{ cm}^{-1}$  in YAG

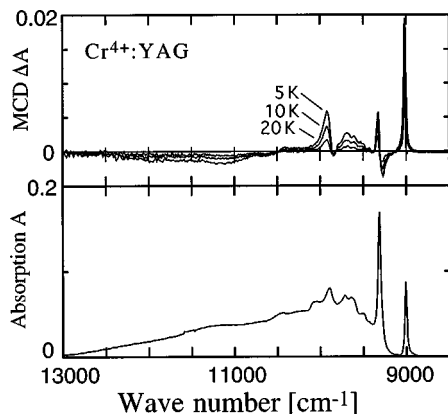


FIG. 2. Near-IR absorption at 5 K (lower) and temperature-dependent MCD (upper) spectra with  $B=5$  T in  $\text{Cr}^{4+}:\text{YAG}$  at the temperatures indicated.

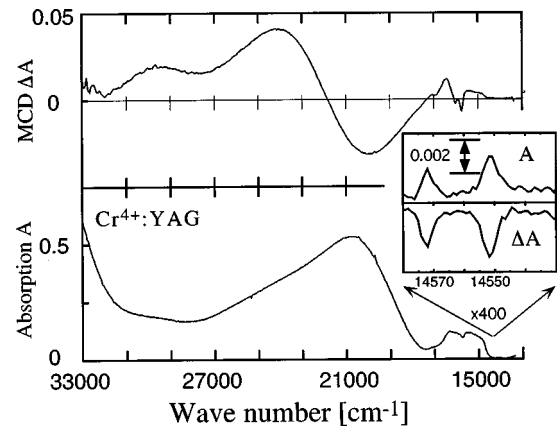


FIG. 3. Visible region absorption (lower) and MCD (upper) at 5 K and  $B=5$  T in  $\text{Cr}^{4+}:\text{YAG}$ . Inset shows the expanded absorption and MCD of the  $R$  line region associated with  $\text{Cr}^{3+}$  at an octahedral site in the sample (see text).

and near  $14500 \text{ cm}^{-1}$  in YGG.<sup>13</sup>

Concentrating on the near-IR region associated with  $\text{Cr}^{4+}$ , there are two sets of distinct origins in both YAG and YGG in Fig. 1; a weak pair near  $\sim 7800 \text{ cm}^{-1}$  and a stronger pair near  $\sim 9000 \text{ cm}^{-1}$ . Linewidths are significantly narrower in YAG. The values for these transitions are given in Table I. The relative sharpness of the  $\text{Cr}^{4+}:\text{YAG}$  spectra is due to the fact that YAG crystals grown by the Czochralski method are ordered, whereas YGG is distorted by a distribution of  $\text{Ga}^{3+}$  ions between  $A$  and  $B$  sites [ $\text{Y}_{3-x}\text{Ga}_{2+x}(\text{GaO}_4)_3$ ]. Since this disorder is random, it leads to the broadening of the spectral features of both the  $\text{Cr}^{4+}$  and  $\text{Cr}^{3+}$  ions.<sup>14</sup>

The selectively excited luminescence spectra of  $\text{Cr}^{4+}:\text{YAG}$  and  $\text{Cr}^{4+}:\text{YGG}$  are shown in Fig. 4. In each case, there appears to be two luminescence sites. Luminescence from both sites is obtained with 780.0-nm excitation, while the lower energy luminescence dominates when 999.8-nm excitation is used. CW excitation at 514 nm with an  $\text{Ar}^+$  laser leads to emission spectra similar to that obtained with 780-nm pulsed excitation. Selective narrowing experiments, exciting with narrow band radiation into the origin feature near  $9000 \text{ cm}^{-1}$  in YAG, showed some slight narrowing of the emission feature near  $7840 \text{ cm}^{-1}$ .

### IV. DISCUSSION

The luminescence of tetrahedral ions in the iso-electronic series  $\text{Fe}^{6+}$ ,  $\text{Mn}^{5+}$ ,  $\text{Cr}^{4+}$  are characterized by a decreasing ligand field.<sup>15</sup> This results in  ${}^1E \rightarrow {}^3A_2$ -type emission in  $\text{Fe}^{6+}$ ,  $\text{Mn}^{5+}$ , and  ${}^3T_2 \rightarrow {}^3A_2$ -type emission in  $\text{Cr}^{4+}$ . For a weak ligand field (small  $Dq$ ), the  ${}^3T_2$  state becomes the lowest excited state and the emitting state. The level crossing of the  ${}^1E/{}^3T_2$  states occurs close to the value of the ligand field strength of the  $\text{Cr}^{4+}$  garnet systems.

The triplet character of the emitting state in  $\text{Cr}^{4+}:\text{YAG}$  has been established by the intensity, lifetime ( $\sim 30 \mu\text{s}$ ) and the existence of a large vibrational sideband characteristic of a  ${}^3T_2$  state. The alternative  ${}^1E \rightarrow {}^3A_2$ -type emission is characterized by a longer lifetime ( $\sim 1 \text{ ms}$ ), a strong zero phonon line with a weak vibrational sideband. It is the large vibrational sideband of the  $\text{Cr}^{4+}:\text{YAG}$  system that makes it attractive as a tunable laser material.

TABLE I. Experimental electronic transition energies and assignments for  $\text{Cr}^{4+}$ :YAG, YGG.

Observed transitions ( $\text{cm}^{-1}$ ) ( $\Delta A/A$ )		$D_{2d}$ assignments <sup>a</sup>	
YAG	YGG	Spinor states	Orbital states
		$\Gamma_5 \rightarrow \Gamma_4$	${}^3B_1$ ZFS
7814 (-) <sup>b</sup>	7511(?)	$\Gamma_5 \rightarrow \Gamma_3$	${}^3B_1({}^3A_2) \rightarrow {}^3B_2({}^3T_2)$
7842 (-) <sup>b</sup>		$\Gamma_5 \rightarrow \Gamma_5$	
8977 (+0.3) <sup>c</sup>	8919 (+0.3) <sup>c</sup>	$\Gamma_5 \rightarrow \Gamma_1$	${}^3B_1 \rightarrow {}^3A_2({}^3T_1)$
9281 (-+0.05) <sup>c</sup>	9140 (-+0.05) <sup>c</sup>	$\Gamma_5 \rightarrow \Gamma_5$	
$\sim 10\,000$ <sup>d</sup>	$\sim 10\,500$ <sup>d</sup>		${}^3B_1 \rightarrow {}^3E({}^3T_2)$
$\sim 15\,650$	$\sim 16\,000$		${}^3B_1 \rightarrow {}^3E({}^3T_1)$

<sup>a</sup>The irreducible representations of the  $D_{2d}$  point group are used to label both orbital and spin-orbital states. The tetrahedral labels are given in brackets.

<sup>b</sup>MCD sign only, absorption feature not observable.

<sup>c</sup>Estimated for  $g\beta B \gg kT$ .

<sup>d</sup>Calculated. The transition is assumed to lie under the vibronic sideband of the  ${}^3B_1({}^3A_2) \rightarrow {}^3A_2({}^3T_1)$  transition.

The  ${}^3A_2 \rightarrow {}^1E$  transition in the absorption spectrum of the  $\text{Cr}^{4+}$ :YAG system has variously been assigned as the first weak doublet ( $\sim 7800 \text{ cm}^{-1}$ ),<sup>16</sup> the second strong doublet ( $\sim 9000 \text{ cm}^{-1}$ ),<sup>5</sup> or to a pair of weak transitions between these ( $\sim 8265 \text{ cm}^{-1}$ ).<sup>6</sup> In this study, we will show that these assignments are incorrect. It is misleading to treat the  ${}^1E$  transition as a doublet in  $\text{Cr}^{4+}$ :YAG as the tetrahedral  ${}^1E$  state will be split by  $>1000 \text{ cm}^{-1}$  by the  $D_{2d}$  distortion.

Notwithstanding their  ${}^1E$  assignment, we do agree with the overall assignments of Eilers *et al.*,<sup>6</sup> which is based on polarized absorption/fluorescence and piezospectroscopy. In exact tetrahedral symmetry the  $\text{Cr}^{4+}$  system is expected to be very close to the cross-over point of the  ${}^3T_2$  and  ${}^1E$  excited states. This is shown schematically in Fig. 5 together with the relationships between the  $T_d$  and  $D_{2d}$  energy levels. The large  $D_{2d}$  distortion splits the  ${}^3T_2$  state into  ${}^3B_2({}^3T_2)$  and  ${}^3E({}^3T_2)$  states; the  ${}^3B_2$  state is then pushed further below the  ${}^1E$  state for a tetragonal elongation of the tetrahedra.

This  ${}^3B_2$  state is then further split by spin-orbit coupling and is seen as a doublet in both the absorption and emission spectra shown in Figs. 1 and 4 at  $7814$  and  $7842 \text{ cm}^{-1}$ . The stronger doublet at  $8977$  and  $9281 \text{ cm}^{-1}$  then corresponds to the spin-orbit split  ${}^3A_2({}^3T_1)$  state that results from the  $D_{2d}$  splitting of the  ${}^3T_1$  state. The other component,  ${}^3E({}^3T_1)$  occurs as a strong peak centered much higher in energy at  $15\,500 \text{ cm}^{-1}$ .

This large  ${}^3A_2({}^3T_1) - {}^3E({}^3T_1)$  splitting of  $\sim 6500 \text{ cm}^{-1}$  is exactly that predicted using a ligand field model (see Secs. IV A and IV B) for a tetragonal distortion of  $\alpha = +5^\circ$  as shown in Fig. 6. The  ${}^3E({}^3T_2)$  state is predicted to be at  $\sim 10\,000 \text{ cm}^{-1}$ , and absorption to this state is hidden underneath the vibronic sideband of the  ${}^3B_1({}^3A_2) \rightarrow {}^3A_2({}^3T_1)$  transition. A summary of assignments for  $\text{Cr}^{4+}$ -doped YAG and YGG is given in Table I. These assignments are required on intensity as well as energy grounds. The transitions resulting from components of the tetrahedral  ${}^3A_2 \rightarrow {}^3T_2$  transition are expected to be very weak as they are electric dipole forbidden, whereas the  ${}^3A_2 \rightarrow {}^3T_1$  transitions are electric dipole allowed. In addition, the polarization intensities in absorption and emission are consistent with the above assignment.<sup>6</sup>

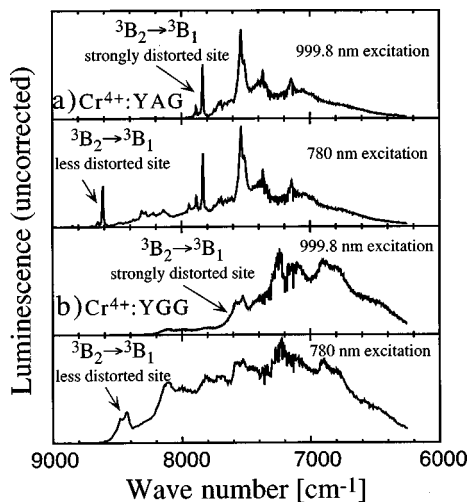


FIG. 4. Selective luminescence spectra excited at the wavelengths indicated at  $T = 1.5 \text{ K}$  of (a)  $\text{Cr}^{4+}$ :YAG and (b)  $\text{Cr}^{4+}$ :YGG. Spectra have not been corrected for system response. Sharp (negative going) features near  $7200 \text{ cm}^{-1}$  are due to atmospheric absorption.

### A. The tetragonal distortion

Figure 6 shows the energy levels resulting from the splitting of the tetrahedral states relative to the ground state, as a

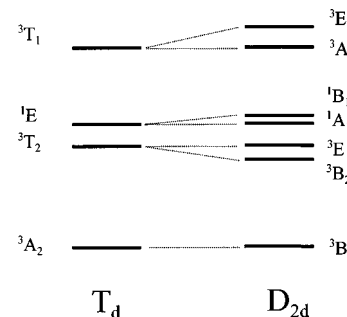


FIG. 5. The schematic energy levels of a  $d^2$  ion in a regular tetrahedral ( $T_d$ ) and elongated tetrahedral ( $D_{2d}$ ) environment. Only levels relevant to the discussion in the text are shown.

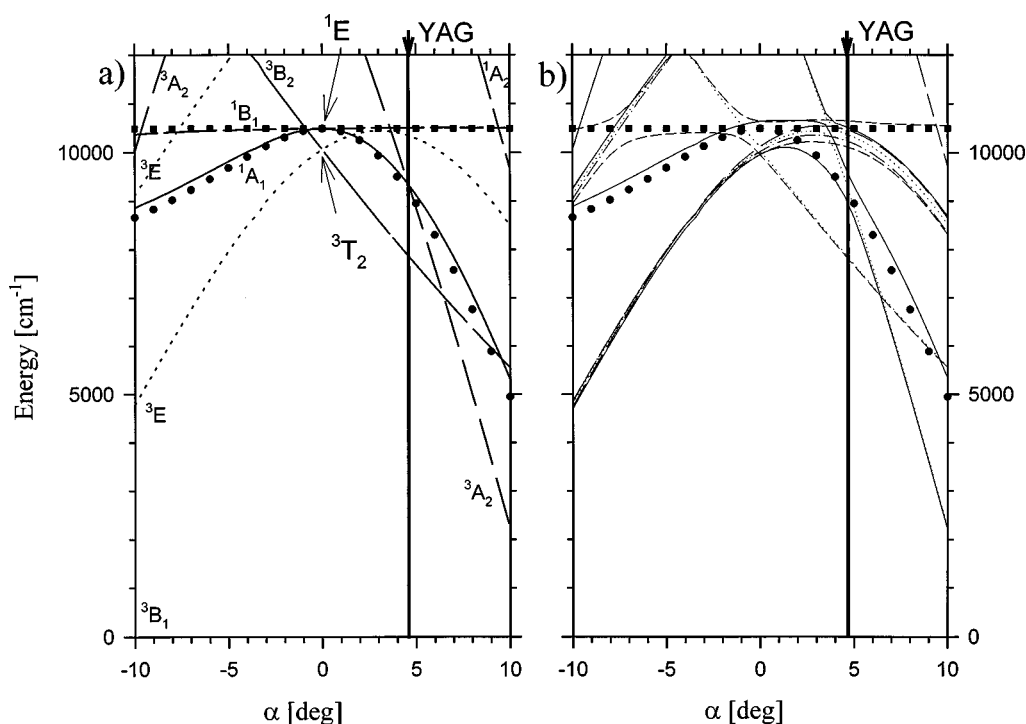


FIG. 6. The low-energy  $d^2$  ligand field levels as a function of the  $D_{2d}$  distortion angle  $\alpha$ ; (a)  $\zeta=0$ , (b)  $\zeta=220\text{ cm}^{-1}$ . Other parameters:  $e_\sigma=13\,585\text{ cm}^{-1}$ ,  $e_\sigma/e_\pi=3$ ,  $B=430\text{ cm}^{-1}$ ,  $C=3575\text{ cm}^{-1}$ . The points indicate the split components of the  ${}^1E$  state using the approximate expressions given in Eqs (2)–(4). In (a) the  $D_{2d}$  ( $T_d$ ) symmetry labels are given for  $\alpha\neq 0$  ( $\alpha=0$ ), respectively.

function of the  $D_{2d}$  distortion of the  $\text{Cr}^{4+}$  tetrahedron. This  $D_{2d}$  distortion is quantified by  $\alpha$ , defined as the angle that each Cr-O bond deviates from tetrahedral and where a positive distortion results in an elongation. In Fig. 6(a) the spin-orbit coupling is set to zero to show the gross behavior of the energy levels as a function of the tetragonal distortion. The energy of the  ${}^3B_2$  component of the  ${}^3T_2$  state drops substantially relative to the ground state as the tetrahedron is elongated. The energy of the  ${}^3B_1({}^3A_2)\leftrightarrow{}^3B_2({}^3T_2)$  transition can be expressed analytically as a function of  $\alpha$  for zero spin-orbit coupling and is given by

$$E({}^3B_2-{}^3B_1)=e_\sigma/3(c^2-2\sqrt{2}sc+1)^2 + e_\sigma/9(7c^4+4\sqrt{2}sc^3-10c^2+4\sqrt{2}sc-1), \quad (1)$$

where  $e_\sigma, e_\pi$  are the angular overlap model (AOM) sigma bonding parameters, which quantify the ligand field<sup>17</sup> and  $s$  and  $c$  denote  $\sin \alpha$ , and  $\cos \alpha$ , respectively. Figure 6(b) shows the same calculation with spin-orbit coupling nonzero. For the values used ( $\zeta=220\text{ cm}^{-1}$ ) the orbital integrity is kept although strong mixing is seen between the  ${}^3A_2({}^3T_2)$  and  ${}^1A_1, {}^1B_1({}^1E)$  states at the  $\alpha\sim 5^\circ$  geometry relevant to this study (Figs. 6 and 7). It is worth noting that neither of the  ${}^1A_1, {}^1B_1({}^1E)$  states become the lowest excited state for any values of  $\alpha$ .

The observed spectral features given in Table I were fitted to a  $d^2$  ligand field calculation by allowing the ligand field ( $e_\sigma, \alpha$ ), spin-orbit coupling ( $\zeta$ ), and interelectron repulsion

parameters ( $B, C$ ) to vary. The calculation used the diagonalization of the full  $d^2$  basis<sup>17</sup> on each iteration of a nonlinear least squares algorithm.<sup>18</sup> The geometry was constrained to  $D_{2d}$  symmetry while the angle  $\alpha$  was allowed to vary, how-

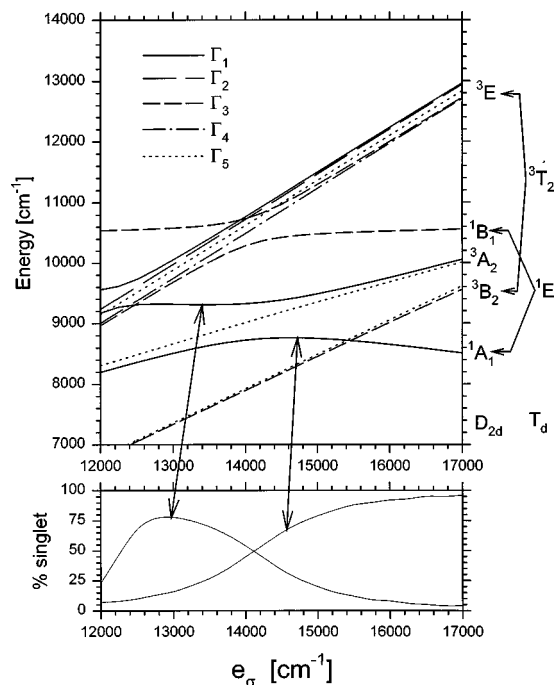


FIG. 7. The  $d^2$  ligand field energy levels near the  ${}^1E/{}^3B_2$  cross over region as a function of the sigma bonding AOM parameter  $e_\sigma$ . The geometry is fixed to that of the YAG host ( $\alpha=4.66^\circ$ ). Other parameters:  $e_\sigma/e_\pi=3$ ,  $B=430\text{ cm}^{-1}$ ,  $C=3575\text{ cm}^{-1}$ ,  $\zeta=220\text{ cm}^{-1}$ . The inset indicates the % singlet character of the two lowest  $\Gamma_1$  states.

TABLE II. The ligand field calculation for  $\text{Cr}^{4+}/\text{YAG}$ . (\*, + indicates states that strongly mix. Parameters used:  $e_\sigma = 15\,585\text{ cm}^{-1}$ ,  $e_\sigma/e_\pi = 3$ ,  $\alpha = 4.66^\circ$ ,  $B = 430.0\text{ cm}^{-1}$ ,  $C = 3585\text{ cm}^{-1}$ ,  $\zeta = 220.0\text{ cm}^{-1}$ .)

Energy ( $\text{cm}^{-1}$ ) ( $D_{2d}^*$ )	$D_{2d}(T_d)$	Observed ( $\text{cm}^{-1}$ )
0.0 ( $\Gamma_5$ )	${}^3B_1({}^3A_2)$	
1.2 ( $\Gamma_4$ )		
7814.6 ( $\Gamma_3$ )	${}^3B_2({}^3T_2)$	7814
7842.6 ( $\Gamma_5$ )		7842
8974.4 ( $\Gamma_1$ )*	${}^3A_2({}^3T_1)$	8977
9278.4 ( $\Gamma_5$ )		9281
9583.0 ( $\Gamma_1$ )*	${}^1E({}^1E)$	~9500
10 652.4 ( $\Gamma_3$ ) <sup>+</sup>		
10 113.9 ( $\Gamma_3$ ) <sup>+</sup>		
10233.3 ( $\Gamma_4$ )	${}^3E({}^3T_2)$	~10 000
10366.2 ( $\Gamma_5$ )		
10459.1 ( $\Gamma_2$ )		
10518.1 ( $\Gamma_1$ )		
15 741.0 ( $\Gamma_4$ )		
15 752.6 ( $\Gamma_3$ )		
15 761.0 ( $\Gamma_1$ )	${}^3E({}^3T_1)$	~15 000
15 771.5 ( $\Gamma_5$ )		
15 796.2 ( $\Gamma_2$ )		
16 927.0 ( $\Gamma_2$ )	${}^1A_2$	
17 672.0 ( $\Gamma_1$ )	${}^1A_1$	
18 280.1 ( $\Gamma_4$ )	${}^1B_2$	

ever it was found that good agreement could be obtained using geometry of the host lattice ( $\alpha = 4.6^\circ$ ). The calculated and experimental transition energies are given in Table II. Differences between calculated and observed energies could be reduced to zero, but the parameters obtained were rounded and the calculation redone. This results in small differences between calculated and observed values in Table II but allows the calculated energies to be reproduced using the quoted parameters.

### B. The splitting of the tetrahedral ${}^1E$ state

As seen in Fig. 6(a), the tetrahedral  ${}^1E$  state splits into  ${}^1A_1$  and  ${}^1B_1$  states in a  $D_{2d}$  tetragonal field. This splitting is essentially independent of the spin-orbit coupling and is predominantly caused by a large off-diagonal coupling between the  ${}^1A_1({}^1E)$  and  ${}^1A_1({}^1A_1)$  states by the tetragonal ligand field. Approximate expressions have been found for the two components  ${}^1A_1, {}^1B_1({}^1E)$ . These are given by

$$E({}^1B_1) = E({}^1E^a), \quad (2)$$

$$E({}^1A_1) = 1/2(E({}^1E^a) - E({}^1A_1^a)) + \{[E({}^1E^a) - E({}^1A_1^a)]^2 + 4\Delta E^2\}^{1/2}.$$

Here,  $E({}^1E^a)$  and  $E({}^1A_1^a)$  are the (exact) orbital energies of the lowest  ${}^1E$  and  ${}^1A_1$  states of a  $d^2$  system in tetrahedral symmetry

$$E({}^1E^a) = 17/2B + 2C + \Delta - \{(7/2B)^2 + B\Delta + \Delta^2\}^{1/2}, \quad (3)$$

$$E({}^1A_1^a) = 17B + 9/2C + \Delta - \{[5/2(2B + C)]^2 + (2B + C)\Delta + \Delta^2\}^{1/2},$$

where  $\Delta = 4/9(3e_\sigma - 4e_\pi)$ .

The symbol  $\Delta E$  in Eq. (2) denotes the energy inequivalence of the  $d_{z^2}, d_{x^2-y^2}$  orbitals due to the tetragonal distortion of the tetrahedral ligand field

$$\Delta E = e_\sigma s^2(7c^2 + 4\sqrt{2}sc + 1) + 4/3e_\pi(7c^4 + 4\sqrt{2}sc^3 - 8c^2 + 1), \quad (4)$$

where  $s = \sin \alpha$  and  $c = \cos \alpha$ .

This expression works well for a large range of  $\alpha$  values and are shown as the points in Figs. 6(a) and 6(b). Even when spin-orbit coupling is introduced, the above approximate expressions correctly span avoided crossings between states that carry the greatest singlet character. As indicated in the diagrams, at  $\alpha = 5^\circ$  the  ${}^1B_1-{}^1A_1$  splitting is some  $\sim 1500\text{ cm}^{-1}$ . The large tetragonal distortion in the host lattice ( $\alpha = 4.66^\circ$ ), which is required to explain the spectral assignments, would also cause a large splitting of the  ${}^1E$  tetrahedral state. It is for this reason that we feel that the assignment of Eilers *et al.*<sup>6</sup> of the  ${}^1E$  to bands at 1206 and 1210 nm is unlikely. However, the singlet character is not well defined in this region due to spin-orbit interaction with the  ${}^3A_2({}^3T_2)$  state. This is shown at the bottom of Fig. 7 where the singlet character of the two relevant  $\Gamma_1$  states changes as they undergo an avoided crossing.

### C. Polarizations and MCD spectra

A number of important experiments have been made by Eilers *et al.*<sup>6</sup> The zero phonon lines of transitions to  $\Gamma_1, \Gamma_5$  of the  ${}^3A_2({}^3T_1)$  state were studied as a function of uniaxial stress. Stress applied parallel to the (001) direction in the lattice caused a splitting of each line due to an orientational rather than intrinsic degeneracy. This is because the  $\text{Cr}^{4+}$  will dope randomly into tetrahedral sites where the elongated axis can be along the  $x, y,$  or  $z$  crystallographic axes. Stress applied parallel to the (111) direction does not result in a splitting as all three sites are equivalent in this direction. This is additional confirmation that the  $\text{Cr}^{4+}$  enters the distorted tetrahedral site of YAG as well as the assignment of these transitions as arising from the  ${}^3A_2$  state.

In addition, the polarization dependent emission was used to assign the emitting state as originating from the  ${}^3B_2({}^3T_2)$  level, based on  $z$ -polarized magnetic dipole selection rules. However, while agreeing with the assignment, we would argue that an  $xy$  electric dipole mechanism dominates the intensity of this transition. Exactly the same polarization behavior for emission is expected in this case and agrees with the experimentally determined sign of the MCD.

With spin-orbit coupling, the  ${}^3B_2({}^3T_2)$  emitting state splits into a  $\Gamma_3$  below a  $\Gamma_5$  (see Table II). The selection rules indicate that the transitions from  $\Gamma_3$  to components of the  ${}^3B_1({}^3A_2)$  ground state are electric dipole allowed in  $xy$  polarization. The transition is also allowed by an  $xy$ -polarized magnetic dipole mechanism, but this will be very weak. The strong  $z$ -polarized magnetic dipole intensity of the  ${}^3T_2$

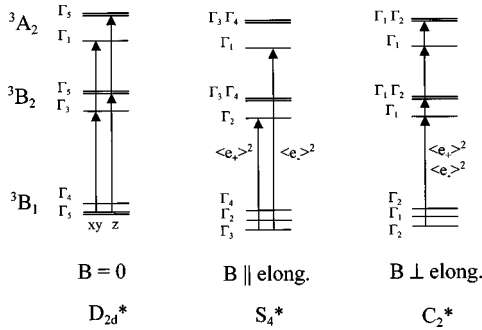


FIG. 8. The energy levels involved in the two pairs of sharp zero phonon lines in different orientations of an applied magnetic field. The left-hand side gives the orbitals states in  $D_{2d}$  symmetry, where the  $\Gamma$  notation for the double point groups is used. Nonzero electric dipole transitions are indicated. For  $B \neq 0$ , the applied magnetic field is directed along  $z$ . In these cases only  $xy$  polarized electric dipole allowed transitions relevant to the MCD are indicated. The  $z$ -polarized electric dipole allowed transitions,  $\Gamma_3 \rightarrow \Gamma_4$  in  $S_4^*$ , and  $\Gamma_2 \rightarrow \Gamma_2$  in  $C_2^*$ , are omitted for clarity.

$\rightarrow {}^3A_2$  tetrahedral transition ends up in the ‘‘hot band’’ emission from the higher energy  $\Gamma_5$  component of the  ${}^3B_2({}^3T_1)$  state.

Excitation with 1064-nm light propagating along (100) and polarized along (001) selectively excites the  ${}^3A_2({}^3T_1)$  state of the sites with the elongation along (001). This site then relaxes to the emitting state. For an  $xy$  electric dipole allowed transition this site will then emit with light polarized along (010) and (100). Light polarized along (100) is observed in the (010) direction. Thus, the origin of the emission is expected to be polarized parallel to the 1064 nm excitation light, as is observed.<sup>6</sup> For excitation with 600–700-nm light propagating along (100) and polarized along (001), the  ${}^3E({}^3T_2)$  state is excited in  $xy$  polarization, selecting the two sites elongated along (100) and (010). In this case relaxation to the emitting state will result in emission with greater intensity polarized *perpendicular* to the excitation, as is observed.<sup>6</sup>

Thus, the emission can be either  $z$  magnetic dipole, or  $xy$  electric dipole allowed to reproduce the behavior of the emission polarizations. However, emission from the lowest excited state ( $\Gamma_3$ ) is magnetic dipole forbidden in  $z$  polarization using the  $D_{2d}^*$  double point group. In addition, the  $xy$  electric dipole mechanism is required to explain the signs of the MCD. For an applied magnetic field parallel to (001) the symmetry of the three  $D_{2d}$  sites are reduced to one of  $S_4^*$  and two of  $C_2^*$  symmetry (for sites with the elongation axis parallel and perpendicular to the applied magnetic field respectively). The energy levels that give rise to the  ${}^3B_2({}^3T_2)$  and  ${}^3A_2({}^3T_1)$  zero phonon lines split in a manner indicated in Fig. 8.

We first consider the  $S_4^*$  site. In the low-temperature limit the electronic selection rules give nonzero transitions to the lower of each doublet. The  $\Gamma_3({}^3B_1) \rightarrow \Gamma_2({}^3B_2)$  transition is completely right circularly polarized,  $e_+ = -1/2(e_x + i e_y)$ , while the  $\Gamma_3({}^3B_1) \rightarrow \Gamma_1({}^3A_2)$  transition is completely left circularly polarized,  $e_- = 1/2(e_x - i e_y)$ . This will contribute to a negative and positive MCD sign to these transitions, respectively, as is seen experimentally (Fig. 1 and Table I). If the magnetic dipole selection rules were used for the

$\Gamma_3({}^3B_1) \rightarrow \Gamma_2({}^3B_2)$  transition, a *positive* MCD would be predicted, contrary to the negative sign observed. The  $S_4^*$  site will not contribute to the MCD of the upper components  $\Gamma_3({}^3B_1) \rightarrow \Gamma_3, \Gamma_4({}^3B_2)$  and  $\Gamma_3({}^3B_1) \rightarrow \Gamma_3, \Gamma_4({}^3A_2)$  of the doublets.

For the two sites in which the elongated axis is perpendicular to the applied field, the situation is more ambiguous. All transitions are  $xy$  electric dipole allowed from the  $\Gamma_2({}^3B_1)$  ground state, except for  $\Gamma_2 \rightarrow \Gamma_2$  transitions. However, the Zeeman splitting of the excited state  $\Gamma_1, \Gamma_2$  pairs are calculated to be split  $< 1 \text{ cm}^{-1}$  in the 5 T applied magnetic field and can be considered degenerate. It is not possible to determine the sign of the MCD of the  $C_2^*$  centers from the selection rules alone. However, the axial MCD of the  $S_4^*$  center determines that the limiting  $\Delta A/A = 2$ , while the transverse MCD of the  $C_2^*$  centers implies  $|\Delta A/A| \ll 2$ . (We use the standard definitions<sup>12</sup>  $\Delta A = \langle e_- \rangle^2 - \langle e_+ \rangle^2$ ;  $A = 1/2[\langle e_- \rangle^2 + \langle e_+ \rangle^2]$ .) The observed  $\Delta A/A$  ratios (Table I) indicate that the  $S_4^*$  sites are dominating the intensity of the zero phonon lines. The MCD sign of these zero phonon lines then confirms the present assignments.

#### D. High pressure luminescence

Recently high-pressure luminescence spectra have been measured for  $\text{Cr}^{4+}:\text{YAG}$  and have been interpreted as due to a  ${}^2T_2 - {}^1E$  crossover.<sup>8</sup> The emitting state becomes blue-shifted with pressure as expected for an increase in the ligand field. At 206 kbar the blue shift ceases and the emission lifetime increases. This indicates that a component of the  ${}^1E$  state, which is insensitive to the ligand field, becomes the lowest excited state.

Figure 7 shows a ligand field calculation as a function of the ligand field parameter  $e_\sigma$  at the fixed geometry of YAG ( $\alpha = 4.66^\circ$ ) with spin-orbit coupling included. An increase of the ligand field simulates the application of external pressure to the  $\text{Cr}^{4+}:\text{YAG}$  system. As has been observed experimentally,<sup>8</sup> at a certain value as the pressure (ligand field) is increased, one component of the  ${}^1E$  state becomes the lowest excited electronic state. For all reasonable values of ligand field parameters, only the  $\Gamma_1$  component of the  ${}^1E$  state can become the emitting state.

#### E. $d$ - $s$ mixing

The  $D_{2d}$  symmetry allows the  $3d_{z^2}$  orbital to mix with the  $4s$  metal orbital. It is known that  $d$ - $s$  mixing sometimes produces large energy shifts.<sup>19</sup> In the present case the  $3d_{z^2}$  orbital will be depressed as a function of  $\alpha$  by an amount

$$E(3d_{z^2}) = -e_{ds}4(s^2 + 2\sqrt{2}sc)^2, \quad (5)$$

where  $e_{ds}$  is a parameter quantifying the  $d$ - $s$  mixing.<sup>19</sup> The above expression gives the correct values of  $E(3d_{z^2}) = 0$  and  $-4e_{ds}$  for the limiting cases of  $\alpha = 0^\circ (T_d)$  and  $\alpha = -35.26^\circ (D_{4h})$ . For distortions of the order  $\alpha \approx 5^\circ$ , the energy shift due to  $d$ - $s$  mixing amounts to  $E(3d_{z^2}) \approx -0.25e_{ds}$ . For  $\text{CuCl}_4^{2-}$  complexes it has been found<sup>19</sup> that  $e_{ds} = 1000 \text{ cm}^{-1}$ , so the effects here will be small.

The  $d$ - $s$  mixing was investigated as a possible reason for the large reduction in the Racah parameter  $B$ , but we con-

clude that  $d$ - $s$  mixing is not important for these systems. Both the  ${}^3B_1({}^3A_2)$  ground state and  ${}^3B_2({}^3T_2)$  first excited state contain the  $d_{z^2}$  orbital so their energy difference is unaffected by  $e_{ds}$ . The  ${}^3A_2({}^3T_1)$  excited state to a first approximation does not contain the  $d_{z^2}$  orbital and so the transition energy will be calculated to be larger if  $e_{ds}$  is included. Since the  ${}^3T_1$  state is at  $\Delta + 12B$  from the ground state in the tetrahedral limit, this would require a further reduction of  $B$ . However, since the effect is likely to be quite small,  $e_{ds}$  mixing was not included in the final fit.

### F. Multiple $\text{Cr}^{4+}$ sites

Although the luminescence for the two sites shown in Fig. 4 can be of comparable intensity, the lower energy luminescence arises from a minority site, its intensity being enhanced by laser selection. This is evident from the absence of comparable absorption features associated with the low-energy site. Luminescence from up to four  $\text{Cr}^{4+}$  sites has been previously observed<sup>8</sup> and it has been suggested that they arise from site perturbation by the  $\text{Ca}^{2+}$  codopant.

The dodecahedral, octahedral, and tetrahedral sites in YAG have the bond lengths 2.38 (av), 1.94, and 1.76 Å respectively. The Ca-O bond length of the  $\text{CaO}_6$  center in CaO is 2.405 Å, so substitution of  $\text{Ca}^{2+}$  at the dodecahedral site would seem most likely. The dodecahedral polyhedra share the short edge of the tetrahedral polyhedra,<sup>10</sup> an increase in the dodecahedral polyhedra from  $\text{Ca}^{2+}$  substitution could possibly increase the short edge of the tetrahedral polyhedra. This would reduce tetragonally elongated distortion and increase the energy of the  $\text{Cr}^{4+}$  emitting state, as observed. In addition, the garnet grossularite ( $\text{Ca}_3\text{Al}_2\text{Si}_3\text{O}_{12}$ ) contains  $\text{Ca}^{3+}$  ions in the dodecahedral site.<sup>10</sup> The presence

of  $\text{Ca}^{3+}$  could also account for some minority sites, as could calcium ions in the next nearest-neighbor positions.

### G. Comparison with previous ligand field parameters

The ligand field parameters  $e_\sigma = 13\,585\text{ cm}^{-1}$ ,  $e_\sigma/e_\pi = 3$  give a cubic ligand field splitting  $\Delta = 4/9(3e_\sigma - 4e_\pi) = 10\,063\text{ cm}^{-1}$ , similar to the values  $9150\text{ cm}^{-1}$  (Ref. 6) and  $10\,667\text{ cm}^{-1}$  (Ref. 5) found previously. The value of  $B = 430\text{ cm}^{-1}$  obtained here is lower than values [ $515\text{ cm}^{-1}$  (Ref. 6) and  $500\text{ cm}^{-1}$  (Ref. 5)] previously given. Our value is  $\sim 43\%$  of the free ion value. This large reduction in the Racah parameters of  $d^2\text{ MO}_4^{x-}$  ions has previously been commented on by many others and is largest in  $\text{FeO}_4^{2-}$  where a reduction to 27% of the free ion value is observed.<sup>20</sup> We have investigated possible explanations for this reduction, which include  $d$ - $s$  mixing and a differential nephelauxetic effect but conclude that neither of these refinements can account for the large reduction. It appears that large covalency effects are present in these systems.

### V. CONCLUSIONS

The MCD and luminescence of the  $\text{Cr}^{4+}$  ion in the  $D_{2d}$  distorted tetrahedral sites of YAG and YGG hosts has been studied. The identification and nature of the different observed sites has been investigated by site selective luminescence. The spectra can be assigned using the geometry of the host lattice, the energies from a ligand field calculation and the polarization and MCD selection rules. A large reduction of the interelectron repulsion ligand field parameter  $B$  from the free-ion value was required. We examine some possible reasons for this and conclude that covalency effects are very important for these tetraoxo ions.

- <sup>1</sup>V. Petricevic, S. K. Gayen, and R. R. Alfano, *Appl. Phys. Lett.* **53**, 2590 (1988).
- <sup>2</sup>A. P. Shkadarevich, in *OSA Proceedings on Tunable Solid State Lasers*, edited by M. L. Shand and H. P. Jenssen (Optical Society of America, Washington, D.C., 1989), Vol. 5, pp. 60–65.
- <sup>3</sup>J. Koetke, S. Kueck, K. Petermann, G. Huber, G. Cerullo, M. Danailov, V. Magni, L. F. Qian, and O. Svelte, *Opt. Commun.* **101**, 195 (1993).
- <sup>4</sup>Y. P. Tong, P. M. W. French, J. R. Taylor, and J. O. Fujimoto, *Opt. Commun.* **136**, 235 (1997).
- <sup>5</sup>S. Kueck, U. Pohlmann, K. Petermann, G. Huber, and T. Schoenherr, *J. Lumin.* **60/61**, 192 (1994).
- <sup>6</sup>H. Eilers, U. Hoemmerich, S. M. Jacobsen, W. M. Yen, H. R. Hoffman, and W. Jia, *Phys. Rev. B* **49**, 15 505 (1994).
- <sup>7</sup>S. Kueck, K. Petermann, U. Pohlmann, and G. Huber, *Phys. Rev. B* **51**, 17 323 (1995).
- <sup>8</sup>Y. R. Shen, U. Hoemmerich, and K. L. Bray, *Phys. Rev. B* **56**, R473 (1997).
- <sup>9</sup>M. A. Scott, Ph.D. thesis, University of Strathclyde, 1995.
- <sup>10</sup>F. Euler and J. A. Bruce, *Acta Crystallogr.* **19**, 971 (1965).
- <sup>11</sup>R. Stranger, L. Dubicki, and E. Krausz, *Inorg. Chem.* **35**, 4218 (1996).
- <sup>12</sup>S. B. Piepho and P. N. Schatz, *Group Theory in Spectroscopy with Applications to Magnetic Circular Dichroism* (Wiley-Interscience, New York, 1983).
- <sup>13</sup>W. A. Wall, J. T. Karpick, and B. Di Bartolo, *J. Phys. C* **4**, 3258 (1971); B. Struve and G. Huber, *Appl. Phys. B: Photophys. Laser Chem.* **36**, 195 (1985).
- <sup>14</sup>M. Yamaga, A. Marshall, K. P. O'Donnell, B. Henderson, and Y. Miyazaki, *J. Lumin.* **39**, 335 (1988).
- <sup>15</sup>M. F. Hazenkamp, H. U. Guedel, S. Kueck, G. Huber, W. Rauw, and D. Reinen, *Chem. Phys. Lett.* **265**, 264 (1997).
- <sup>16</sup>K. R. Hoffman, U. Hoemmerich, S. M. Jacobsen, and W. M. Yen, *J. Lumin.* **52**, 277 (1992).
- <sup>17</sup>M. Gerloch, *Magnetism and Ligand Field Analysis* (Cambridge University Press, Cambridge, 1983).
- <sup>18</sup>R. P. Brent, *Algorithms for Minimization without Derivatives* (Prentice Hall, Englewood Cliffs, NJ, 1973).
- <sup>19</sup>M. J. Riley, *Inorg. Chim. Acta* **268**, 55 (1998).
- <sup>20</sup>M. F. Hazenkamp, H. U. Guedel, M. Atanasov, U. Kesper, and D. Reinen, *Phys. Rev. B* **53**, 2367 (1996).